Journal of Structural Geology, Vol. 11, No. 7, pp. 847 to 858, 1989
Printed in Great Britain

0191-8141/86 $03.00 + 0.00
Pergamon Press plc

Dynamic recrystallization in semi-brittle faults

FREDERICK M. CHESTER*

Center for Tectonophysics and Department of Geophysics,
Texas A & M University, College Station, TX 77843, U.S.A.

(*Received* 4 *November* 1988; *accepted in revised form* 3 *April* 1989)

Abstract—Experiments designed to investigate the microstructure and mechanical behavior of shear zones across the cataclastic faulting to dislocation creep transition indicate that some mylonites may be the products of frictional faulting under semi-brittle conditions. The experiments involve simple shear of thin layers of polycrystalline halite to strains (γ) of 5–8, at temperatures to 250°C, normal stresses to 90 MPa and at shear strain rates of 7×10^{-3} s^{-1}. Microstructural and mechanical data define a transitional field of semi-brittle flow. Steady-state stress in the semi-brittle field is a function of the normal stress and the temperature, and is significantly less than that predicted by the power-law equation used to describe dislocation creep, and by the friction law used to describe cataclastic faulting. Fracture and localized slip are characteristic processes in the fields of cataclastic faulting and semi-brittle flow, whereas intracrystalline plasticity, recovery and dynamic recrystallization are characteristic of semi-brittle flow and dislocation creep. For both semi-brittle flow and dislocation, creep migration recrystallization is activated only after a critical strain and temperature–stress condition are achieved. The recrystallized grain size is consistent with previously established piezometric relations for dislocation creep. These experiments indicate that the field of semi-brittle flow for halite is characterized by frictional behavior even though the corresponding microstructure primarily reflects microscopic plastic deformation and softening processes.

INTRODUCTION

FRICTIONAL behaviour is characterized by a strong dependence of shear strength on normal stress, and is typical of faulting by cataclastic mechanisms (e.g. Sibson 1977, Paterson 1978). However, frictional behavior is not necessarily restricted to brittle faulting. Deformation associated with frictional slip in metals is almost entirely crystal-plastic (Bowden & Tabor 1964). Rock deformation experiments have shown that the strength of simulated faults may depend on normal stress even if strain is achieved primarily through mechanisms of crystal-plasticity or solution-transfer (Dula 1985, Shimamoto & Logan 1986, Chester & Logan in press). These findings support the suggestion that some mylonitic shear zones are the products of frictional faulting under semi-brittle conditions (Shimamoto & Logan 1986, Scholz 1988).

The purpose of this paper is to present the results of experiments designed to investigate the microstructure of shear zones across the transition from frictional to pressure-insensitive creep behavior. The experiments involve shear of thin layers (0.5 mm thick) of polycrystalline halite between blocks of quartzose sandstone at normal stresses from 10 to 90 MPa, temperatures from 22 to 250°C and at a shear displacement rate of 7×10^{-3} mm s^{-1} (nominal shear strain rate of 7×10^{-3} s^{-1}) in a triaxial rock deformation apparatus (Fig. 1). The range of conditions is sufficient to cause a change from deformation by primarily cataclastic mechanisms to deformation by dislocation creep.

The present experiments are part of an ongoing study of the friction and flow properties of polycrystalline halite in shear (Fig. 2). Previous experiments, all done at room-temperature, show that at sufficiently high confining pressures (greater than 100 MPa) and low shear strain rates (less than 10^{-4} s^{-1}), shear strength is insensitive to normal stress (Shimamoto & Logan 1986). For halite, this behavior probably represents low-temperature (exponential) creep by dislocation-dominated mechanisms (Chester 1988a). At lower normal stresses, differences in mechanical behavior and microstructure define two distinct fields of frictional faulting referred to as cataclastic faulting and semi-brittle flow (Chester 1988a, Chester & Logan in press). Cataclastic faulting occurs at the lowest normal stresses and can be described by a friction constitutive law with a coefficient of friction between 0.6 and 1.0. The microstructure in the cataclastic faulting field suggests that deformation is dominantly brittle. Semi-brittle flow also exhibits frictional behavior, but produces a microstructure indicative of dominantly crystal-plastic deformation and recrystallization (Shimamoto & Logan 1986, Knapp *et al.* 1987).

The changes in mechanical behavior of halite across the transition from cataclastic faulting to dislocation creep should be representative of other minerals because all deform by the same basic processes of cataclasis and crystal-plasticity (e.g. Carter 1976, Paterson 1978). Of course this analogy is not completely rigorous because rock forming minerals have different crystal structure and bonding (e.g. Frost & Ashby 1982). Nevertheless the previous shear experiments on halite at room temperature illustrate the general characteristics of the transition from cataclastic faulting to low-temperature (exponential) creep. Because the high deviatoric stresses required for exponential creep are

*Present address: Lamont-Doherty Geological Observatory of Columbia University, Palisades, NY 10964, U.S.A.

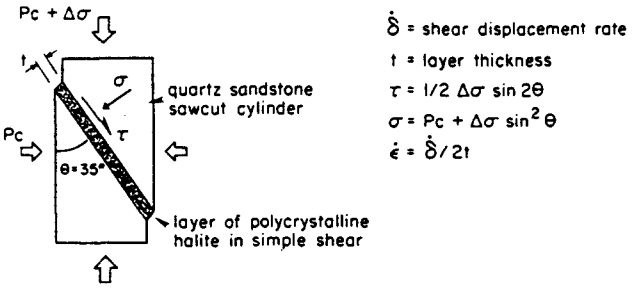

Fig. 1. Specimen configuration for triaxial shear experiments. Thin layers (thickness t) of halite are sheared at shear displacement rate ($\dot{\delta}$) between blocks of quartzose sandstone under confining pressure (P_c) and differential axial stress ($\Delta\sigma$). Positive normal stress (σ), shear stress (τ) and the nominal shear strain rate ($\dot{\varepsilon}$) used to characterize mechanical behavior are defined.

probably rarely achieved in natural deformations (Carter & Tsenn 1987), the transition to exponential creep may not be geologically significant. The more significant transition, from cataclastic faulting to high-temperature (power-law) creep, is investigated in the present experiments by conducting tests at low normal stresses and elevated temperatures.

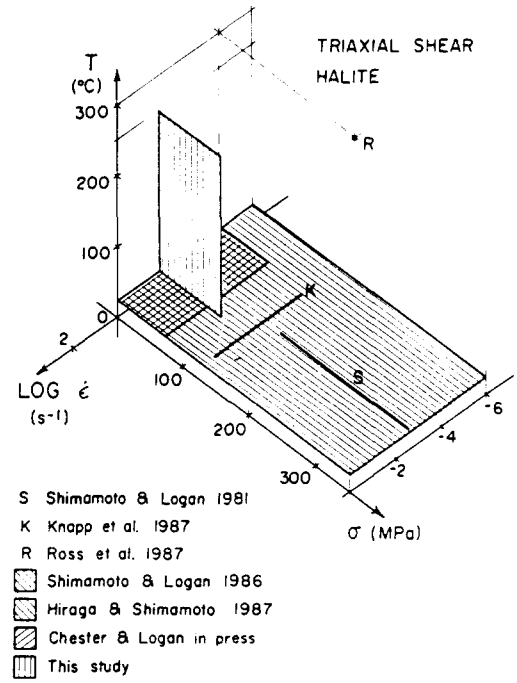

Fig. 2. Temperature, normal stress and strain rate conditions of this study and previous studies of polycrystalline halite in shear.

EXPERIMENTAL METHOD

The halite layers are approximately 0.5 mm thick, and consist of 0.52 ± 0.005 grams of granular, reagent-grade halite with grain diameters between 0.25 and 0.35 mm. The halite is sandwiched between a sawcut cylinder of Coconino sandstone 18.3 mm in diameter (Fig. 1). The sawcut is oriented at 35 ± 0.1° to the cylinder axis, and the surfaces are lapped with 220 grit silicon carbide. The specimen is jacketed in lead and copper, and shortened under confining pressure in a liquid confining-media, gear-driven, triaxial apparatus (Heard 1963, Chester 1988b). Axial shortening of the specimen causes shear of the halite layer; the sandstone is not permanently deformed. Except during the first increments of deformation when the halite layer undergoes some compaction, the layer is deformed in simple shear.

The accuracy of measurements with the testing apparatus is as follows: confining pressure to within 0.16 MPa; axial displacement of the apparatus piston to within 0.5% of the total; axial force inside the pressure vessel to within 1% of the total; temperature to within 2°C. Temperature differences across the specimen are less than 1% of nominal.

The stress state during shear is defined in terms of the average normal stress (σ) and shear stress (τ) acting on the plane of the layer. The shear stress, normal stress and shear displacement are calculated by computer during the experiment from measurements of confining pressure, axial force and axial displacement of the piston (Chester 1988b). Calculation of shear displacement requires corrections for the elastic distortion of the apparatus from confining pressure and differential axial load. The values of shear strain (γ) and shear strain rate ($\dot{\varepsilon}$) reported assume that deformation in the layer is homogeneous. Calculation of the shear and normal stresses assumes stress in the specimen is homogeneous, and involves corrections for strength of the jacketing and for the decrease (with slip) in cross-sectional area of the specimen that supports the differential load. Calculated values of stress are probably accurate to within several percent of the total value.

The halite is sheared at constant normal stresses by varying the confining pressure during the experiment. In several tests the constant normal-stress shearing was preceded with a confining pressure (P_c) reduction load path (Shimamoto & Logan 1986, Chester & Logan in press). The P_c-reduction load path involves reduction of confining pressure after establishing a differential axial load on the specimen, and imposes approximately 0.5 mm shear displacement on the layer. The P_c-reduction load path is used to reduce the shear displacement necessary to achieve steady-state behavior in halite at low normal stresses. It has little effect on the mechanical behavior at the other conditions tested (Chester & Logan in press).

Before and after the experiments the specimens were stored with desiccant in a sealed container at 22°C and 2% relative humidity. The deformed specimens were saturated with epoxy cement and cut into petrographic sections that were oriented perpendicular to the halite layer and parallel to the shear direction. Deodorized kerosene was used as lubricating agent for polishing and cutting the sections. The sections were etched and studied optically under reflected and transmitted light.

RESULTS

Mechanical behavior

Thirty-seven experiments at different normal stress and temperature conditions were successful (Table 1).

Table 1. Experimental results

Experiment No.	Normal stress (MPa)	Temperature (°C)	Total shear displacement (mm)	SS—steady state WH—work hardening WS—work softening	Shear displacement to steady-state (mm)	Final shear stress (MPa)
10*	25 to 40	22	3.0	stick–slip to WH	—	44
12*	24	75	2.6	SS	1.4	27
13*	24	50	2.4	SS	1.4	26
14	36	150	3.8	SS	2.0	28
15	30	125	3.4	SS	1.0	28
16	50	125	3.1	SS	1.5	36
17	40	125	3.0	SS	1.2	32
18	50	75	3.0	SS	1.8	45
19	70	125	3.6	SS	2.3	40
20	20	125	2.6	WS	>2.0	21
21	90	125	3.6	SS	2.5	39
22	90	75	3.8	WH	>3.2	55
23	10	125	2.5	SS	0.9	10
24	70	75	3.8	SS	2.8	51
25	40	75	3.0	SS	1.4	36
26	10	75	2.4	SS	0.7	10
27	70	22	3.6	SS	2.5	49
28*	20	32	2.8	WS	>2.2	24
29	30	75	3.5	WS	>2.9	33
30	30	175	2.9	SS	1.0	23
31	30	225	3.0	SS	0.4	16
32	70	175	3.2	SS	1.0	25
33	70	225	3.0	SS	0.3	17
35	20	200	2.6	SS	0.9	15
36	10	225	2.5	SS	0.8	8
37	10	175	2.0	SS	0.0	10
38	40	200	3.0	SS	0.5	21
39	90	200	3.2	SS	0.7	21
40	30	50	3.2	WS	>3.0	28
41	20	75	2.5	SS	1.4	22
42	40	150	3.1	SS	1.3	30
43	90	150	3.5	SS	1.7	34
44	50	100	3.3	SS	1.5	43
45	40	50	3.1	WS	>2.9	39
46	90	100	3.8	WH	>3.4	53
47	20	250	2.5	SS	0.2	14
48†	50	125	2.0	SS	0.4	19‡

0.5 mm thick layers of reagent grade halite sheared at constant normal stress and 7.0×10^{-3} mm^{-1} shear displacement rate.
*With 70 MPa P_c-reduction load path.
†6.7×10^{-5} mm s^{-1} shear displacement rate.
‡With rate correction for jacket strength.

In all experiments, the halite layers yielded at a small shear displacement (less than 0.5 mm) and except for experiment No. 10, were stable (Fig. 3). In most cases the halite work-hardened to a steady-state shear stress. The halite shear zones were said to achieve steady-state if the shear stress did not vary more than ±0.5 MPa during the final 1.0 mm of shear displacement. Based on this criterion, halite layers in 29 of the experiments achieved steady-state, two work-hardened, five work-softened and one displayed stick–slip behavior (Table 1).

Reproducibility was not checked directly; however, the relative strengths and shearing behavior of all experiments are internally consistent (Fig. 3). Moreover, the mechanical response of two tests conducted at room-temperature is consistent with previous experiments conducted at the same conditions but in a different apparatus (Chester & Logan in press). The shear stress vs shear displacement curves indicate that the progressive misalignment of the specimen halves with displacement, which produces a maximum change in cross-sectional area of 15%, does not affect the shear behavior (Fig. 3).

Shear strength

The steady-state shear strength varies systematically over the range of normal stress and temperature conditions tested. As would be expected, shear stress increases with increasing normal stress at a constant temperature and decreases with increasing temperature at a constant normal stress (Fig. 3). The greatest shear stresses are achieved at lower temperatures and higher normal stresses. The magnitude of the final shear stress in experiments that work-harden or work-soften is consistent with the trends suggested by the experiments that achieve a steady-state shear stress (Table 1).

The shear displacement necessary to achieve steady-state also varies systematically with normal stress and

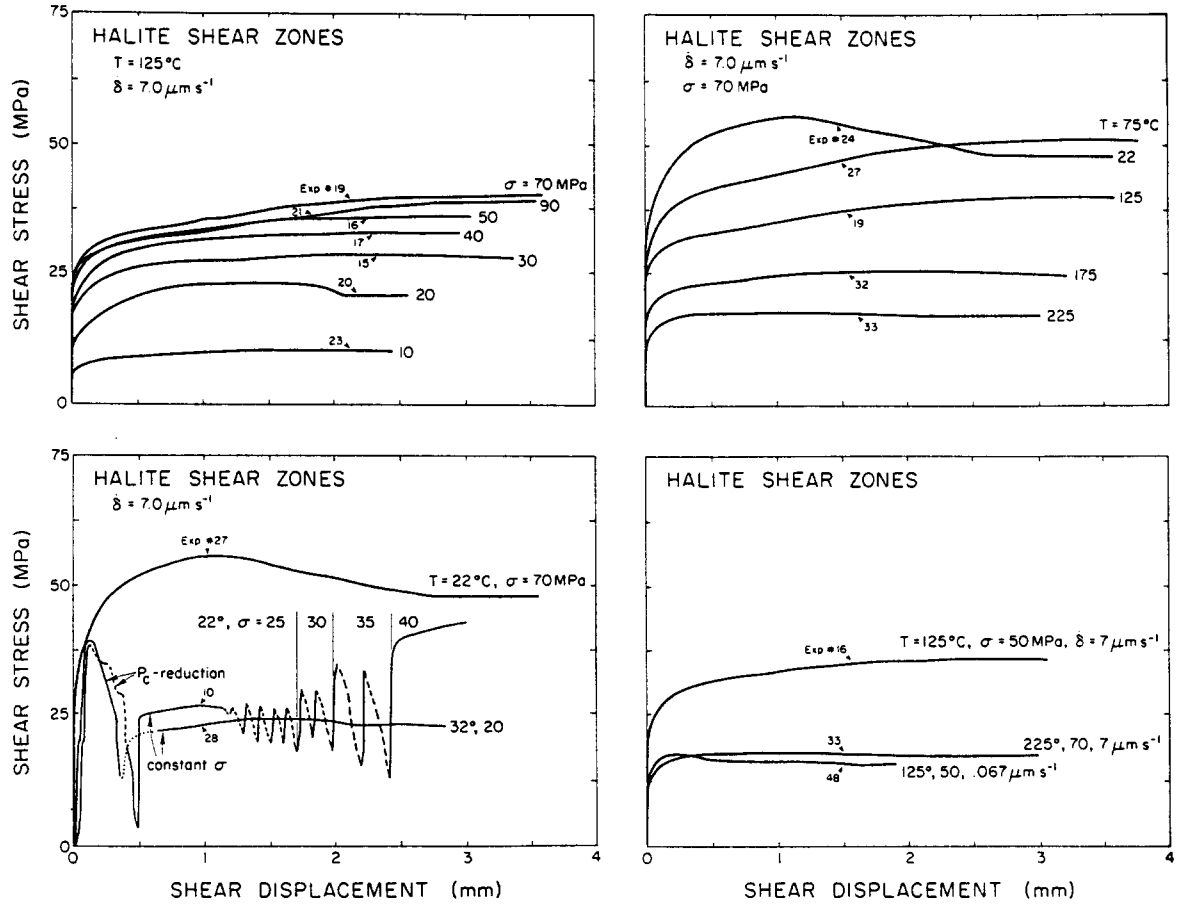

Fig. 3. Shear stress versus shear displacement records of representative experiments. Test conditions and experiment number are indicated.

temperature, and appears to approximately correlate with the magnitude of the steady-state shear stress (Table 1). Normal stress and temperature conditions that produce a higher steady-state shear stress also require greater shear displacements to achieve steady-state. The two experiments that work-harden at all displacements also achieve the highest final shear stress. Work-softening does not appear to correlate with the magnitude of shear stress.

The steady-state shear stress of the experiment (No. 48) conducted at a lower shear-displacement rate of 6.7 $\times 10^{-5}$ mm s^{-1} is less than that of the experiment (No. 16) at the same temperature and normal stress conditions but at the standard displacement rate (Fig. 3). The mechanical response of the low displacement rate test is quite similar, however, to a standard displacement rate test at greater temperatures (No. 33, Fig. 3).

Temperature sensitivity of instability

The experiment run at 22°C and 20 MPa normal stress exhibited unstable shearing behavior (No. 10, Fig. 3). In this test the normal stress was increased stepwise to document an unstable to stable shearing transition at a normal stress of 40 MPa. At the same temperature, but at a normal stress of 70 MPa, stable slip occurred (No. 27, Fig. 3). These results are consistent with previous findings that the stability transition at room temperature occurs at a normal stress of 40 MPa. Comparison of these results with an experiment at a normal stress of 20 MPa and temperature of 32°C indicates that an increase in temperature can suppress instability. All of these low-temperature and low normal stress experiments employed a P_c-reduction load path. The effect of temperature can also be seen during P_c-reduction; unstable shear behavior occurs during P_c-reduction at 22°C but not at 32°C (Fig. 3).

Mechanism fields

Based on the mechanical behavior of halite as a function of normal stress and temperature, we can define the fields of deformation for three mechanisms: cataclastic faulting, semi-brittle flow and dislocation creep (Fig. 4). The same fields were defined in the room-temperature data set based on the variation in microstructure and mechanical behavior with normal stress and shear displacement rate (Chester 1988a, Chester & Logan in press).

In the cataclastic faulting field at low normal stresses and temperatures, the steady-state shear strength depends on normal stress, which is adequately expressed by a constant coefficient of friction of 1.0. This correlates with the behavior observed at low displacement rates and room-temperature. Increasing temperature at constant normal stress has little effect on the strength in this

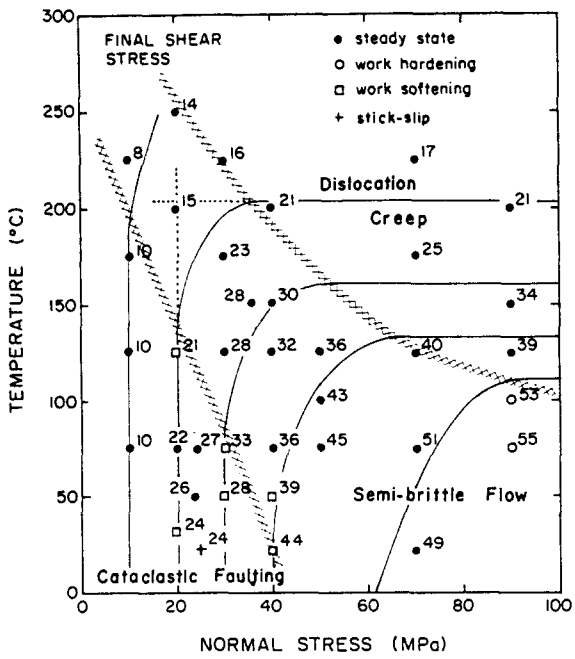

Fig. 4. Final shear stress as a function of the temperature and normal stress conditions of experiments from Table 1. Thin lines are contours of shear stress, and show graphically the dependence of strength on normal stress and temperature. Contours are essentially vertical in the cataclastic faulting field and indicate little sensitivity of shear stress to temperature. Contours are horizontal in the dislocation creep field and indicate no sensitivity of shear strength to normal stress. Inclined contours in the field of semi-brittle flow indicate a dependence on both normal stress and temperature. The functional relationships for either dislocation creep or cataclastic faulting overestimate shear strength if extrapolated into the field of semi-brittle flow, as shown by the dotted lines for a shear stress of 20 MPa. The mechanical behavior delineates three deformation-mechanism fields. Approximate boundaries of the mechanism fields are indicated with hatched lines, and may be defined in terms of the normal stress and the dislocation creep stress as described in the text.

field, but does cause a change from stick–slip to stable shearing. At constant room-temperature, decreasing shear displacement rate causes a similar change in stability (Chester & Logan in press). These observations suggest that increasing temperature has the same effect on rate-dependent frictional behavior and stability as decreasing displacement rate. Such behavior is expected for frictional slip involving thermally activated mechanisms following an Arrhenius relationship (Chester 1988c).

At the highest normal stresses and temperatures, steady-state shear strength is a function of temperature but not normal stress (Fig. 4), which is consistent with flow by dislocation creep. Fitting the experimental data from this field above 150°C to the power-law creep equation $\dot{\varepsilon} = A \exp[-Q/RT]\tau^n$, where Q is the apparent activation energy for creep, n is the stress exponent, R is the gas constant and A may be approximated as a constant (e.g. Carter 1976), suggests that Q/Rn is approximately 1900 K. Comparison of these data with the flow strength of the experiment (No. 48) conducted at a lower strain rate suggests n is approximately 5.5 and Q is approximately 8.7×10^4 J mol^{-1} (Chester 1988b). These values are consistent with previous determinations of Q and n for dislocation creep in reagent-grade, polycrystalline halite (Heard 1972, Heard & Ryerson 1986). Shear in the dislocation-mechanism field at temperatures below 150°C probably occurs by low-temperature (exponential) creep (Chester 1988a), as found in the experiments conducted at low strain rates and high normal stresses by Shimamoto & Logan (1986).

At intermediate conditions, steady-state flow strength depends on normal stress and temperature. The steady-state stress is significantly less than would be predicted by extrapolation of the mechanical behavior from either the dislocation creep or cataclastic faulting fields (Fig. 4). This distinguishes a mechanism field of semi-brittle flow that extends the same field documented at room-temperature (Chester 1988a). The boundaries of the semi-brittle flow field can be defined in terms of the normal stress and the steady-state stress for dislocation (power-law) creep (τ_c). The boundary with dislocation creep is approximately defined by $\sigma = 2\tau_c$, and the boundary with cataclastic faulting by $\sigma = \tau_c/2$.

Microstructure

The microstructure of the sheared halite was documented in 12 experiments (Table 2). Shearing causes intragranular flow, microfracturing and recrystallization (Fig. 5). The relative occurrence of fractures and recrystallization varies systematically with normal stress and temperature, and correlates with the mechanically defined mechanism fields (Fig. 7).

In each experiment the microstructure varies along the layer, particularly within 1 mm of the perimeter of the layer. This latter variation reflects the inhomogeneous stress and strain conditions produced by misalignment of specimen halves in the triaxial configuration. Observations reported are from the interior portion of the layers.

Two general types of microfractures are distinguished: those formed during shearing (shear fractures) and those formed after shearing, during the cooling and unloading stage (unloading cracks). The unloading cracks typically are open, oriented subparallel to the layer and easily distinguishable.

The microfractures formed during shearing show components of shear and normal separation and are concentrated within small domains (Fig. 5). They are preferentially oriented at small angles to the layer in the orientation of R_1 Riedel shears (e.g. Logan *et al.* 1979). The shear fractures are formed only in the fields of cataclastic faulting and semi-brittle flow (Fig. 7), and their orientation does not vary systematically with temperature or normal stress. The magnitude of separation normal to the fracture (dilation) and the associated brecciation decrease with increasing normal stress and temperature, whereas the spacing between domains of shear fractures increases with normal stress and temperature (Fig. 5, Table 2).

Grain structure is evident in reflected light due to the preferential etching of high-angle grain boundaries. That shearing produces recrystallization is evinced by the reduction in grain size, and the formation of grain

Table 2. Microstructure and recrystallized grain size

Experiment No.	Shear strain (γ)	Mechanism field*	Number of zones of shear fracture	Large recrystallized grains	
				Extent of recrystallization	Log $\bar{d}$† (μm)
27	7.2	S	several	partial	1.39 ± 0.38
41	5.0	C	many	incipient	not measured
25	6.0	C/S	1–2	partial	1.64 ± 0.25
24	7.6	S	1	partial	1.42 ± 0.24
44	6.6	S	2–3	partial	1.49 ± 0.22
46	7.6	S/D	none	complete	1.55 ± 0.18
20	5.2	C/S	several	partial	not measured
43	7.0	D	none	complete	1.62 ± 0.17
30‡	5.8	S/D	1–2	partial	1.76 ± 0.20
35	5.2	S/D	1	partial	1.84 ± 0.17
38	6.0	D	none	complete	1.82 ± 0.19
39	6.4	D	none	complete	1.84 ± 0.17

*C, cataclastic faulting; D, dislocation creep; S, semi-brittle flow.
†$\bar{d}$ is the mean grain diameter from measurements of the long and short axes of grains in this section, 25 grains measured for each experiment.
‡Log $\bar{d}$ of small recrystallized grain set is 0.45 ± 0.27.

boundaries in new material positions (Figs. 5a & e and 6). Although the recrystallized grain size varies both within and between halite layers, two sets of recrystallized grains can be distinguished by their relative size. In samples where both sets are present, the mean grain size of one set is greater than that of the other by a factor of approximately 20 (Fig. 6).

Complete recrystallization to the larger grain size occurs in the field of dislocation creep (Fig. 7 and Table 2). Semi-brittle flow produces both large and small grain sets. The cataclastic faulting field is characterized by incipient recrystallization, primarily to the larger grain size.

The shapes of single, isolated, large recrystallized grains within strained original grains, or within a domain of smaller recrystallized grains, are both euhedral and irregular (Fig. 6). The size and structure of the large grains suggest that they formed by the migration of high-angle boundaries of strain-free grains through areas of high strain energy (Guillopé & Poirier 1979, Urai *et al.* 1986). Recrystallization to the large grain size destroys all evidence of the structure of the starting material. In the domains where this process has gone to completion, grain boundaries often are planar and intersect at 120°, although curved, irregular boundaries and intersection angles of 90–180° are present (Fig. 6). The mean grain size increases with a decrease in shear stress (Table 2). Etching reveals that some of the large grains are polygonized (Fig. 6).

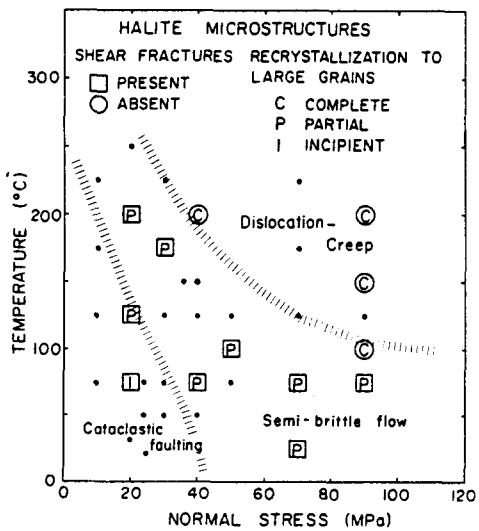

Fig. 7. Microstructure of halite as a function of temperature and normal stress and with respect to the mechanism fields defined by mechanical behavior.

Recrystallization to the finer grain size is most apparent in the field of semi-brittle flow. If present, the small grains occur in pods, rather than evenly dispersed throughout the layer. The pods often are associated with zones of shear fracture (Fig. 6). The small grains occur in ribbons which define a shape foliation (S-foliation) that has the opposite sense of obliquity to the layer as the shear fractures (Fig. 6). The mean size of the small grains appears to increase with a decrease in shear stress, although this is difficult to document optically because grain size is often less than 1 μm. The grain size of this set is similar to the subgrains in both the large recrystallized grains and in the strained, original grains.

Planar arrays of fluid inclusions are spatially associated with the fine-grain set and shear fractures, and are approximately parallel to the S-foliation. These planar arrays terminate in the interiors of the large recrystallized grains, away from the shear fractures. The planar arrays generally are absent within the polygonized, original grains, and in domains that are completely recrystallized to the coarse-grain set. Fluid inclusions are present, however, along the boundaries of the large recrystallized grains.

Some of the original grain boundaries of the granular starting material are evident after shear in the field of cataclastic faulting by virtue of the lack of recrystallization. A faint S-foliation also is produced in this field by the reorientation of the grain boundaries through distributed intragranular shear (Fig. 5). The sheared original grains are polygonized (Fig. 6), which indicates crystal-plastic mechanisms were operative at the lowest temperatures and normal stresses tested.

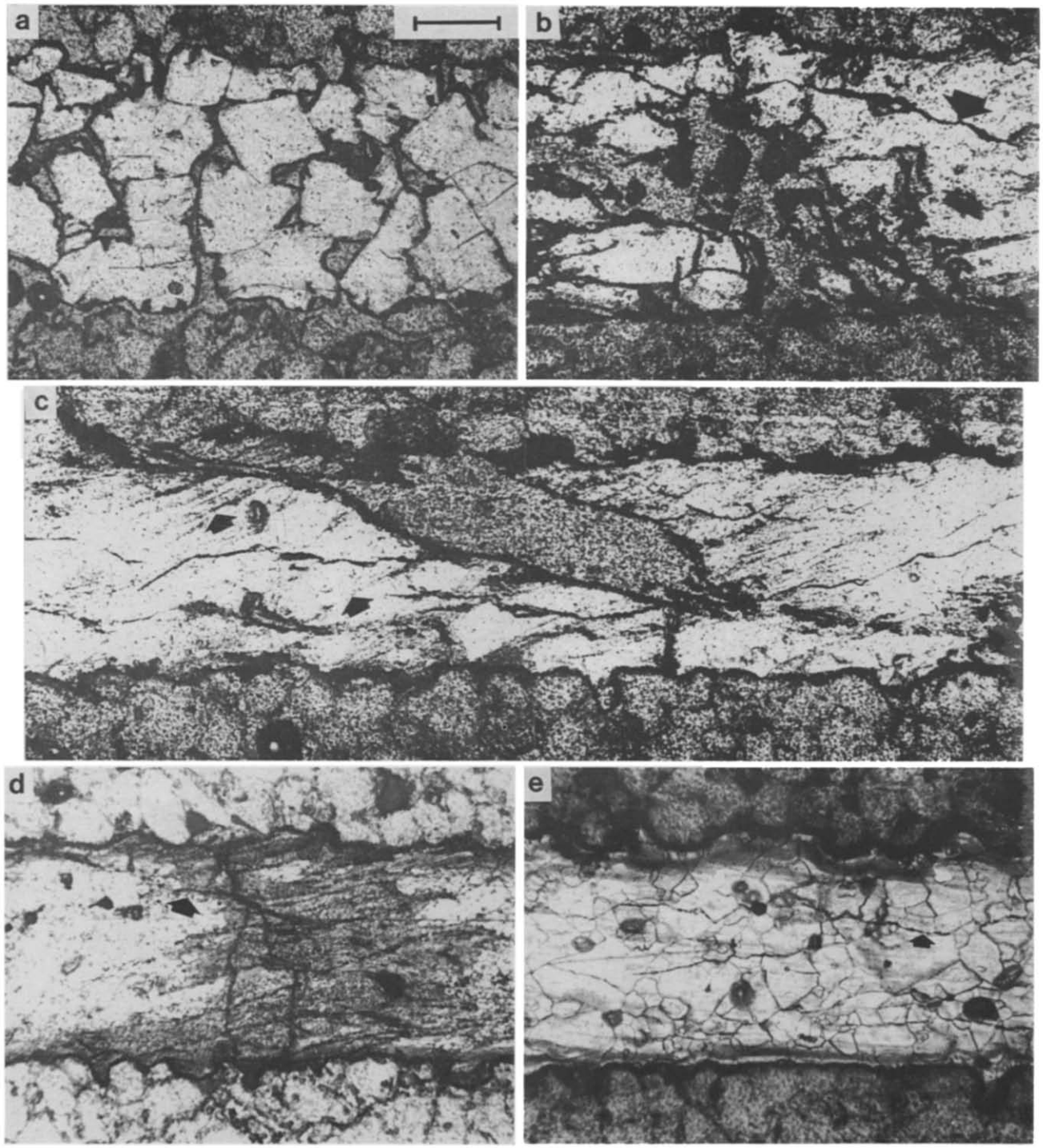

Fig. 5. Microstructure of halite sheared at different normal stresses and temperatures across the cataclastic faulting to dislocation creep transition. In all views the halite layer is in the center of the photograph, bounded by sandstone, and oriented for right-lateral shear. Scale bar is 0.2 mm; transmitted light unless noted otherwise. (a) Starting structure of halite layer subjected to a 70 MPa confining pressure but no shear displacement (exp. No. 2404, Chester & Logan in press). Cubic halite grains are slightly deformed and layer is compacted, although significant porosity is retained. (b) Shear fracture and associated brecciation characteristic of the field of cataclastic faulting at slightly elevated temperatures (exp. No. 41). Unloading crack is identified with arrow. (c) Shear fracture characteristic of the boundary between cataclastic faulting and semi-brittle flow at a low normal stress (exp. No. 20). Note the lack of brecciation and the termination of the oblique, dilatant fracture into layer-parallel cataclastic zones at the sandstone–halite interface. A faint *S*-foliation (arrows) is defined by fluid inclusions and grain boundaries in the interior of the layer near the fracture. (d) View under reflected light showing shear fracture (arrow) and *S*-foliation characteristic of the field of semi-brittle flow (exp. No. 30). *S*-foliation has the opposite sense of obliquity as the shear fracture. The vertical fractures are unloading cracks. Light areas (more reflective) are halite recrystallized to larger grains. Darker areas (less reflective) near the shear fracture are domains of small recrystallized grains. (e) View under reflected light showing halite that has been completely recrystallized to large grains during shear in the field of dislocation creep (exp. No. 39). Note the absence of any evidence of fracture except for the unloading cracks (arrow).

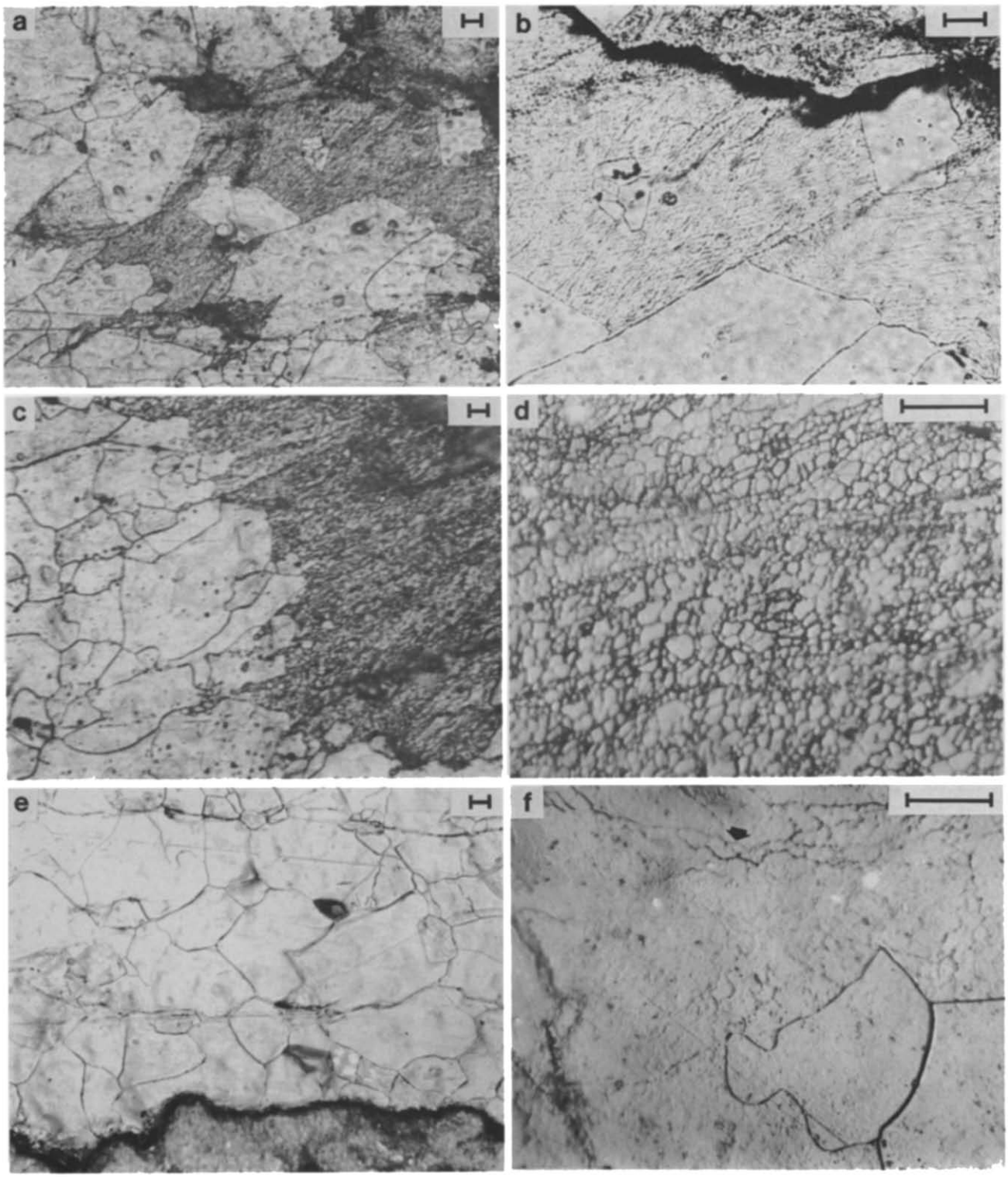

Fig. 6. Microstructures of recrystallized halite. All photographs are under reflected light, unless noted otherwise, and are oriented with the horizontal axis parallel to the boundary of the layer and for right-lateral shear; scale bars are 0.05 mm. (a) Recrystallization by grain-boundary migration in strained, original grains. Planar arrays of dislocations in the original grains are revealed by etching. Both irregular-shaped and euhedral grains are produced by boundary migration. (b) Enlarged view of (a) in transmitted light revealing an unloading crack transecting a euhedral, recrystallized grain. (c) Domains of large and small recrystallized grains in a layer sheared in the field of semi-brittle flow (exp. No. 20). The mean diameter of large grains is approximately 20 times that of the small recrystallized grains. (d) Small recrystallized grains. Shape fabric of individual grains and sets of grains define the *S*-foliation. (e) Portion of layer completely recrystallized to the larger grain size (exp. No. 39). Grain boundaries are approximately planar and intersect at approximately 120°. In these recrystallized domains fluid inclusions are located primarily along grain boundaries. (f) Example of subgrains (arrow) within large recrystallized grains. Subgrain grain size is similar to the small recrystallized grains.

DISCUSSION

The correlation between mechanical behavior and microstructure in all of the halite experiments substantiates the distinction of independent mechanism fields based on the mechanical behavior (Chester 1988a, Chester & Logan in press). The formation of shear fractures and the frictional behavior indicate cataclastic processes are operative, at least to a limited extent, in the field of cataclastic faulting and semi-brittle flow. The microstructure also suggests that crystal-plastic mechanisms are operative throughout all fields. Shear in the fields of semi-brittle flow and dislocation creep causes significant intragranular strain and recrystallization. Recrystallization is an important softening process, and can influence the relative importance of plastic and brittle mechanisms at steady-state. Important questions for each mechanism field are, how do the brittle and plastic mechanisms interact and contribute to the total strain, and how significant are softening processes during shear?

Static recrystallization

The recrystallization to euhedral grain shapes implies that the recrystallization occurred during the final stages of deformation or after shearing, as it is unlikely that these shapes would be preserved if the halite was subjected to additional shear strain. However, the recrystallization to euhedral grains must have been completed shortly after shearing, prior to the reduction of confining pressure, because unloading cracks cut these grains (Fig. 5). In the elevated temperature experiments the confining pressure is not reduced until the specimen cools. This provides several hours for static recovery; a significantly greater time than that of the actual shearing experiment. The formation of euhedral grains cut by unloading cracks was also observed in room-temperature shearing tests by Knapp *et al.* (1987). In these tests no cooling was necessary, and the time between the end of shearing and reduction of confining pressure was only minutes. Some of the tests of Knapp *et al.* (1987) were conducted at low strain rates and were sheared for many hours. All of these data suggest essentially instantaneous nucleation and growth of the recrystallized grains, and that some recrystallization probably also occurred during shear (i.e. was dynamic).

Static recrystallization immediately after deformation involving dynamic recrystallization (metadynamic recrystallization, McQueen & Jonas 1975) was noted by Guillopé & Poirier (1979) for creep of halite at very high temperatures and observed *in situ* for wet salt rocks by Urai (1983). In these two cases the static recrystallization proceeds because sufficient energy is stored in the deformed grains to cause continued migration of high-angle grain boundaries (e.g. Urai *et al.* 1986). Based on analogy with recrystallization in ceramics, Urai (1983) suggested that the growth of euhedral shapes in wet salt rocks during metadynamic recrystallization could reflect the presence of a small amount of water along grain boundaries. Although the experiments of the present study were conducted nominally dry, some water must have been present and could have been important in producing the euhedral shapes.

Dynamic recrystallization

Dynamic recrystallization in halite and most other minerals occurs by two basic processes: rotation recrystallization involving the progressive misorientation of polygonized grains (by dislocation climb and recovery) to form new grains with high-angle boundaries and migration recrystallization involving the motion of high-angle grain boundaries (e.g. Guillopé & Poirier 1979, Tullis & Yund 1985, Urai *et al.* 1986). Mechanisms of recrystallization may be further distinguished in terms of the relative contribution and temporal continuity of microstructural transformation by these two processes (e.g. Drury *et al.* 1985, Tullis & Yund 1985, Urai *et al.* 1986). Halite undergoing high-temperature creep is characterized by continual polygonization and rotation recrystallization with some slow migration of grain boundaries (Carter & Hansen 1983, Guillopé & Poirier 1979). However, Guillopé & Poirier (1979) documented that if a critical strain is achieved (approximately 60% coaxial shortening) and if conditions of the experiments exceed a critical temperature–stress condition, rapid migration of grain boundaries may occur and transform the microstructure to larger, strain-free grains. This is consistent with the common observation from coaxial creep experiments that only polygonization and rotation recrystallization occur in halite (e.g. Carter & Hansen 1983) because typically only small strains are achieved.

The bimodal grain size distribution of recrystallized grains noted in the elevated-temperature experiments reported here also was noted in the room-temperature shear experiments on halite by Knapp *et al.* (1987). Their tests, to sequential shear strains (γ) between 1 and 15, document that growth of the larger grains does not occur until permanent shear strains of 2–3 are achieved. This is consistent with the critical strain for migration recrystallization determined by Guillopé & Poirier, as shear strains of 3 are approximately equivalent in magnitude to 70% coaxial shortening (e.g. Schmid *et al.* 1987). Knapp *et al.* (1987) also document that a mosaic of fine grains is formed prior to growth of the coarse grains. This progression appears analogous to that documented by Guillopé & Poirier (1979), in which small recrystallized grains form first by rotation recrystallization, followed by growth to larger grain sizes by migration recrystallization. Presumably, the same progression of recrystallization in the experiments by Knapp *et al.* (1987) and Guillopé & Poirier (1979) occurs in the experiments here.

The observations of halite sheared beyond the critical strain ($\gamma = 3$) for migration recrystallization, as indicated in Fig. 7, suggest that the extent of recrystallization to the larger grain size is a function of temperature and normal stress. These define an empirical temperature–stress critical condition for migration re-

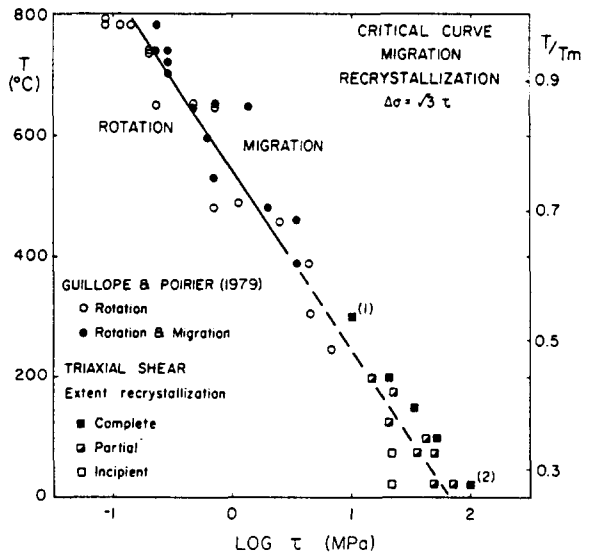

Fig. 8. Conditions over which migration recrystallization occurs in temperature vs log shear stress space. Observations of Guillopé & Poirier (1979, table 1) at high homologous temperature and low stress, and the results of the shear experiments, imply a critical temperature–stress condition for migration recrystallization. Differential stress ($\Delta\sigma$) in coaxial creep tests of Guillopé & Poirier are compared with shear stress (τ) in triaxial shear tests through the second invariant of deviatoric stress. Observations labeled (1) and (2) are from experiments by Ross *et al.* (1987) and Shimamoto & Logan (1986), respectively.

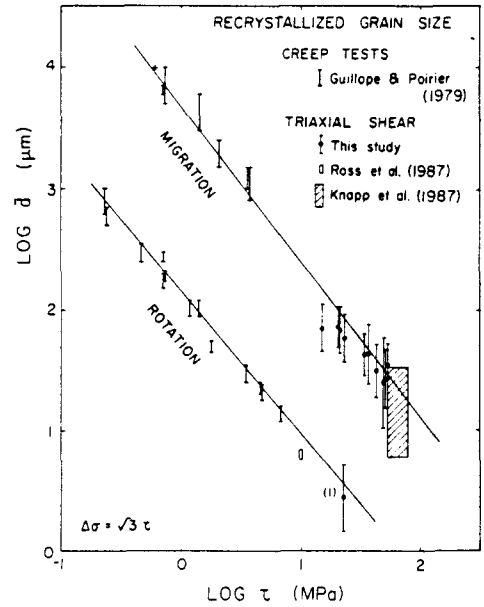

Fig. 9. Log–log plot of mean recrystallized grain size ($\bar{d}$) vs shear stress for halite. Sizes of the large and small recrystallized grains in the shear tests are consistent with the observations and piezometric relations (lines) of Guillopé & Poirier (1979, table 1 and equations 2 and 3) for migration and rotation recrystallization during high-temperature creep in halite. Observations of this study show mean and standard deviation as listed in Table 2. Data point labeled (1) correlates to the size of the fine grain set in experiment No. 30. Grain size observations of other workers show the range of sizes reported. Stress in coaxial creep tests and triaxial shear tests are related as in Fig. 8, although agreement between the data sets is equally good if the shear stress in the triaxial tests is equated with the maximum shear stress ($\Delta\sigma/2$) in the coaxial creep tests.

crystallization that is consistent with the findings of Guillopé & Poirier at more elevated temperatures and lower stresses (Fig. 8). In temperature vs log shear–stress space, the critical curve is approximately linear over 3 orders of magnitude of stress and over a T/T_m between 0.3 and 1.0. Although the creep test data of Guillopé & Poirier (1979) and shear test data may be comparable in terms of temperature and deviatoric stress, other experimental conditions differ. For a specified temperature, different stresses in the creep tests were achieved by changing strain rate, whereas different stresses in the shear tests were achieved by changing normal stress.

Relationships between deviatoric stress and the steady-state microstructure during creep, such as free dislocation density and polygonized and recrystallized grain size, have been documented (Twiss 1977, Carter *et al.* 1982). For halite, the most common relation reported is that the subgrain size is inversely proportional to differential stress (Carter *et al.* 1982). By virtue of the high strains achieved in their creep tests, Guillopé & Poirier (1979) were able to quantify relations between stress and the size of grains produced by the different processes of rotation and migration recrystallization. The mean grain size of the coarse and fine sets produced in the shear experiments are functionally related to deviatoric stress consistent with Guillopé's and Poirier's findings for dynamic recrystallization (Fig. 9). This relationship was not identified in previous shear experiments on halite. Apparently, recrystallized grain size is affected by the presence of segregated impurities in the starting material, large variations in shear strain and operation of static recrystallization well after the experiments (Shimamoto & Lugan 1986, Hiraga & Shimamoto 1987, Knapp *et al.* 1987).

The structure of the larger grains is compatible with dynamic recrystallization as demonstrated by *in situ* studies of recrystallization in rock analogues (e.g. Means 1983, Urai *et al.* 1986). Moreover, the fact that some of the coarse grains are themselves polygonized is consistent with the occurrence of migration recrystallization prior to the end of shearing (Guillopé & Poirier 1979).

Deformation mechanisms

The complete recrystallization of halite by grain-boundary migration at the highest temperatures and normal stresses of the dislocation creep field, where mechanical behavior is consistent with power-law creep, suggests that the flow mechanism at these conditions is combined recovery- and recrystallization-accommodated dislocation creep. Presumably, halite sheared in this field undergoes recrystallization to a fine-grain size by rotation processes initially, and is subsequently transformed to a coarse-grained aggregate by rapid grain-boundary migration. It is less certain what the recrystallization processes are once the layer is completely recrystallized to the large, strain-free grains. It may undergo additional cycles of rotation recrystallization followed by boundary migration, or it may simply undergo continuous grain-boundary migration, similar to octachloropropane (Means 1983).

At lower temperatures in the dislocation creep field, the steady-state shear stress is well above that for power-law breakdown (Tsenn & Carter 1987). Shear experiments by Shimamoto & Logan (1986) at low strain rates and high normal stresses also define a high-stress, low-temperature creep field. All these data can be described with a single exponential creep function typical of the power-law breakdown, low-temperature creep regime (Chester 1988a,b). The microstructure of the halite sheared at steady-state in the low-temperature creep field is the same as in the high temperature creep field. Creep experiments (that are all coaxial) on other rock-forming minerals in the low-temperature creep regime do not typically achieve steady-state and do not produce dynamic recrystallization, but this may simply reflect the fact that these experiments do not achieve the critical strain for recrystallization (e.g. Sellars 1978, Guillopé & Poirier 1979). Dynamic recrystallization during low-temperature creep has been noted for some metals (e.g. Sellars & Tegart 1966, Glover & Sellars 1973).

Based on the deformed shapes of the original halite grains, the fairly uniform orientation of the *S*-foliation, and the preferred crystallographic orientation of the halite (e.g. Knapp *et al.* 1987), Chester & Logan (in press) concluded that crystal-plasticity is the dominant deformation mechanism at room temperature in the semi-brittle field. Microstructures produced in the semi-brittle field at elevated temperatures document that significant softening occurs at steady-state by both recovery and recrystallization, consistent with deformation by crystal-plastic mechanisms. The softening by recrystallization counteracts the hardening associated with crystal-plasticity, and can allow dislocation generation and motion to continue at steady-state. Nonetheless, the flow stress at a given temperature and strain rate in the semi-brittle field is less than that expected if hardening is counteracted only by recovery and recrystallization, as occurs in the dislocation creep field. Presumably, at the lower normal stress conditions of semi-brittle flow, the dislocation density is sufficiently high that the grain-scale stress concentrations can propagate intragranular and intergranular microfractures and generate voids. In fact, void generation during recrystallization dominated ductile flow has been observed in octachloropropane (Ree 1988). Void generation should limit the deviatoric stresses in the aggregate as a function of normal stress and could explain the frictional behavior observed for this field.

Microstructures indicate that both crystal-plasticity and cataclasis occur in the cataclastic faulting field (Chester & Logan in press), but the shapes of grains and the orientation of the *S*-foliation imply only a small portion of the total shear displacement is accommodated by intragranular plasticity. Most of the crystal-plastic deformation occurs at low strains during compaction and reduction of porosity; at which stage the grains are relatively unstrained and thus the critical resolved shear stress for glide is relatively low. Once compacted and hardened, cataclasis dominates and displacements are accommodated by slip along shear fractures and near the boundaries of the layers. Although incipient recrystallization is observed in some cases, it is apparently insufficient to soften the layer or promote continued accommodation of strain by plastic mechanisms. Exceptions to this generalization may be indicated by the mechanical data from experiments near the boundary between cataclastic faulting and semi-brittle flow, which show mechanical softening at high strains (Table 1). This boundary may be near the critical stress–temperature conditions required for recrystallization.

Several aspects of recrystallization in the cataclastic faulting and semi-brittle flow fields may reflect heterogeneous stress conditions within the layers. For example, the layers sheared in the semi-brittle flow field undergo migration recrystallization everywhere but near the shear fractures. It may be that in these regions the stresses are relaxed by fracture to values below the average stress and below the critical stress necessary for migration recrystallization. Similarly, if variation in stress occurs in the halite layers sheared in the cataclastic faulting field, then stress levels in some regions may be sufficient to promote plasticity and recrystallization even though the bulk of the layer experiences brittle deformation.

CONCLUSIONS

(1) An increase in temperature causes a change in mechanisms from cataclastic faulting to dislocation creep. The change in mechanisms is not abrupt, but gradational over a field of semi-brittle flow.

(2) Steady-state flow stress in the semi-brittle field is significantly less than that predicted by extrapolation of relations from the cataclastic faulting and dislocation creep fields, or that predicted if both dislocation creep and cataclastic faulting operated concurrently but independently.

(3) The boundaries of the semi-brittle flow field may be defined in terms of the normal stress and the steady-state creep stress.

(4) The microstructure produced by dislocation creep suggests that dynamic recrystallization by grain-boundary migration is an important softening process at high strains. The microstructures produced in the other mechanism fields indicate that the conditions over which dynamic recrystallization occurs are greater in extent than the conditions for high-temperature (power-law) creep.

(5) Within the frictional regime both cataclastic and crystal-plastic mechanisms operate. Cataclastic faulting is characterized by limited recovery and shear fracturing, dilation and brecciation. Semi-brittle flow is characterized by dynamic recovery and recrystallization, and shear fracturing with relatively small dilation.

(6) Dynamic recrystallization in the field of semi-brittle flow produces a bimodal grain size distribution, which appears to represent products of rotation and migration recrystallization processes. The recrystallized grain size satisfies previously established piezometric

relations for dislocation creep. Also consistent with previous work, migration recrystallization is only activated after a critical shear strain and a critical temperature–stress condition are achieved.

Acknowledgements—Comments by J. G. Spray, W. D. Means, J.-H. Ree, J. Tullis, J. S. Chester and the *Journal* reviewers are appreciated. The experimental phase of this study was partially supported by the National Science Foundation under grant EAR8513615 awarded to J. M. Logan, and through a Graduate Fellowship to the author from the Center for Tectonophysics of Texas A & M University. The observational phase was supported through a Postdoctoral Fellowship from the Lamont-Doherty Geological Observatory of Columbia University.

REFERENCES

Bowden, F. P. & Tabor, D. 1964. *The Friction and Lubrication of Solids, Part II.* Oxford University Press, London.

Carter, N. L. 1976. Steady state flow of rocks. *Rev. Geophys. & Space Phys.* **14**, 301–360.

Carter, N. L. & Hansen, F. D. 1983. Creep of rocksalt. *Tectonophysics* **92**, 275–333.

Carter, N. L., Hansen, F. D. & Senseny, P. E. 1982. Stress magnitudes in natural rock salt. *J. geophys. Res.* **87**, 9289–9300.

Carter, N. L. & Tsenn, M. C. 1987. Flow properties of continental lithosphere. *Tectonophysics* **136**, 27–63.

Chester, F. M. 1988a. The brittle–ductile transition in a deformation-mechanism map for halite. *Tectonophysics* **154**, 125–136.

Chester, F. M. 1988b. The transition from cataclasis to intracrystalline plasticity in experimental shear zones. Unpublished Ph.D. Dissertation, Texas A & M University.

Chester, F. M. 1988c. Temperature and rate dependence of friction for faults (abstract). *EOS Trans. Am. geophys. Un.* **68**, 1464.

Chester, F. M. & Logan, J. M. In press. Frictional faulting in polycrystalline halite: correlation of microstructure, mechanisms of slip and constitutive behavior. In: *The Heard Volume* (edited by Durham, W. B. *et al.*). *Am. Geophys. Un. Geophys. Monogr.*

Drury, M. R., Humphreys, F. J. & White, S. H. 1985. Large strain deformation studies using polycrystalline magnesium as rock analogue. Part II: dynamic recrystallization mechanisms at high temperatures. *Phys. Earth & Planet Interiors* **40**, 208–222.

Dula, W. F., Jr. 1985. High temperature deformation of wet and dry artificial quartz gouge. Unpublished Ph.D. Dissertation, Texas A & M University.

Frost, H. J. & Ashby, M. F. 1982. *Deformation-mechanism Maps: The Plasticity and Creep of Metals and Ceramics.* Pergamon Press, Oxford.

Glover, G. & Sellars, C. M. 1973. Recovery and recrystallization during high-temperature deformation of alpha-iron. *Met. Trans.* **4**, 765–775.

Guillopé, M. & Poirier, J. P. 1979. Dynamic recrystallization during creep of single-crystalline halite: an experimental study. *J. geophys. Res.* **84**, 5557–5567.

Heard, H. C. 1963. Effect of large changes in strain rate in the experimental deformation of Yule Marble. *J. Geol.* **71**, 162–195.

Heard, H. C. 1972. Steady-state flow in polycrystalline halite at pressure of 2 kilobars. In: *Flow and Fracture of Rocks* (edited by Heard, H. C., Borg, I. Y., Carter, N. L. & Raleigh, C. B.). *Am. Geophys. Un. Geophys. Monogr.* **16**, 191–209.

Heard, H. C. & Ryerson, F. J. 1986. Effect of cation impurities on steady-state flow of salt. In: *Mineral and Rock Deformation: Laboratory Studies—The Paterson Volume* (edited by Hobbs, B. E. & Heard, H. C.). *Am. Geophys. Un. Geophys. Monogr.* **36**, 117–160.

Hiraga, H. & Shimamoto, T. 1987. Textures of sheared halite and their implications for the seismogenic slip of deep faults. *Tectonophysics* **144**, 69–86.

Knapp, S. T., Friedman, M. & Logan, J. M. 1987. Slip and recrystallization of halite gouge in experimental shear zones. *Tectonophysics* **135**, 171–183.

Logan, J. M., Friedman, M., Higgs, N. G., Dengo, C. & Shimamoto, T. 1979. Experimental studies of simulated gouge and their application to studies of natural fault gouge. In: *Analysis of Actual Fault Zones in Bedrock* (edited by Speed, R. C. & Sharp, R. V.). *U.S. geol. Surv. Open-file Report* **79–1239**, 276–304.

McQueen, H. J. & Jonas, J. J. 1975. Recovery and recrystallization during high-temperature deformation. In: *Plastic Deformation of Materials* (edited by Arsenault, R. J.). *Treatise on Materials Sci. Tech.* **6**, 394–493.

Means, W. D. 1983. Microstructure and micromotion in recrystallization flow of octachloropropane: a first look. *Geol. Rdsch.* **72**, 511–528.

Paterson, M. S. 1978. *Experimental Rock Deformation: The Brittle Field.* Springer, Berlin.

Ree, J.-H. 1988. Evolution of deformation-induced grain boundary voids in octachloropropane. *Geol. Soc. Am. Abs. w. Prog.* **20**, 213.

Ross, J. V., Bauer, S. J. & Hansen, F. D. 1987. Textural evolution of synthetic anhydrite–halite mylonites. *Tectonophysics* **140**, 307–326.

Schmid, S. M., Panozzo, R. & Bauer, S. 1987. Special Research Paper. Simple shear experiments on calcite rocks: rheology and microfabric. *J. Struct. Geol.* **9**, 747–778.

Scholz, C. H. 1988. The brittle–plastic transition and the depth of seismic faulting. *Geol. Rdsch.* **77**, 319–329.

Sellars, C. M. 1978. Recrystallization of metals during hot deformation. *Phil. Trans. R. Soc. Lond.* **A288**, 147–158.

Sellars, C. M. & Tegart, W. J. McG. 1966. On the mechanism of hot deformation. *Acta metall.* **14**, 1136–1138.

Shimamoto, T. & Logan, J. M. 1981. Effects of simulated fault gouge on sliding behavior of Tennessee sandstone: non-clay gouges. *J. geophys. Res.* **86**, 2902–2914.

Shimamoto, T. & Logan, J. M. 1986. Velocity-dependent behavior of simulated halite shear zones: an analogue for silicates. In: *Earthquake Source Mechanics* (edited by Das, S., Boatwright, J. & Scholz, C. H.). *Am. Geophys. Un. Geophys. Monogr.* **37**, 49–63.

Sibson, R. H. 1977. Fault rocks and fault mechanisms. *J. geol. Soc. Lond.* **133**, 191–213.

Tsenn, M. C. & Carter, N. L. 1987. Upper limits of power law creep of rocks. *Tectonophysics* **136**, 1–26.

Tullis, J. & Yund, R. A. 1985. Dynamic recrystallization of feldspar: a mechanism for ductile shear zone formation. *Geology* **13**, 238–241.

Twiss, R. J. 1977. Theory and applicability of recrystallized grain size paleopiezometry. *Pure & Appl. Geophys.* **115**, 224–227.

Urai, J. L. 1983. Water assisted dynamic recrystallization and weakening in poly-crystalline bischofite. *Tectonophysics* **96**, 125–157.

Urai, J. L., Means, W. D. & Lister, G. S. 1986. Dynamic recrystallization of minerals. In: *Mineral and Rock Deformation: Laboratory Studies—The Paterson Volume* (edited by Hobbs, B. E. & Heard, H. C.). *Am. Geophys. Un. Geophys. Monogr.* **36**, 161–199.